

# UCLA

## UCLA Previously Published Works

### Title

Acetylene Semi-Hydrogenation on Intermetallic Ni-In Catalysts: Ni Ensemble and Acetylene Coverage Effects from a Theoretical Analysis

### Permalink

<https://escholarship.org/uc/item/5nx5h57d>

### Journal

ACS Catalysis, 13(11)

### ISSN

2155-5435

### Authors

Almisbaa, Zahra  
Aljama, Hassan A  
Almajnoui, Khalid  
[et al.](#)

### Publication Date

2023-06-02

### DOI

10.1021/acscatal.3c01175

### Supplemental Material

<https://escholarship.org/uc/item/5nx5h57d#supplemental>

### Copyright Information

This work is made available under the terms of a Creative Commons Attribution-NonCommercial-NoDerivatives License, available at <https://creativecommons.org/licenses/by-nc-nd/4.0/>

Peer reviewed

# Acetylene Semi-Hydrogenation on Intermetallic Ni-In Catalysts: Ni Ensemble and Acetylene Coverage Effects from a Theoretical Analysis

Zahra Almisbaa<sup>1</sup>, Hassan A. Aljama<sup>2</sup>, Khalid Almajnouni<sup>2</sup>, Luigi Cavallo<sup>3</sup> and Philippe Sautet<sup>1,4\*</sup>

<sup>1</sup>*Department of Chemical and Biomolecular Engineering, University of California, Los Angeles, Los Angeles, California 90095 (United States)*

<sup>2</sup>*Research & Development Center, Saudi Aramco, Dhahran 31311 (Saudi Arabia)*

<sup>3</sup>*King Abdullah University of Science and Technology, Thuwal 23955 (Saudi Arabia)*

<sup>4</sup>*Department of Chemistry and Biochemistry, University of California, Los Angeles, Los Angeles, California 90095 (United States)*

\* sautet@ucla.edu (corresponding author)

DFT-based reaction profiles and microkinetic simulations were used to describe the catalytic selective hydrogenation of acetylene on Ni, Ni<sub>3</sub>In, NiIn, and Ni<sub>2</sub>In<sub>3</sub> model intermetallic surfaces. Among the Ni<sub>x</sub>In<sub>y</sub> intermetallic catalysts, NiIn showed the highest ethylene yield. Decreased formation of ethane was observed on NiIn and Ni<sub>2</sub>In<sub>3</sub> accompanied by increased formation of oligomers compared to Ni and Ni<sub>3</sub>In. This emphasizes the significance of accounting for the oligomerization reactions when evaluating the selectivity of the catalysts. Inconsistent acetylene coverage was obtained when performing microkinetic simulations using free energy values calculated at low acetylene coverage, while a fully consistent coverage was obtained using high coverage free energy values. Results from the high coverage microkinetic model showed that the presence of In on the catalytic surface decreased the rate of acetylene consumption with a trade-off relation between activity and selectivity. Simulations in the absence of ethylene in the feed confirmed that ethylene hydrogenation and acetylene C-C coupling were the primary sources for ethane and oligomers formation respectively. This study highlights the importance of considering oligomerization reactions, coverage effect, and feed composition when describing the activity and the selectivity of catalysts during the competitive hydrogenation of alkynes.

## 1. INTRODUCTION

Naphtha steam cracking is one of the primary sources of ethylene production.<sup>1</sup> Ethylene streams that come from steam crackers are the building blocks for polyethylene products and other key polymers. Acetylene is present in ethylene streams at levels of 1% and must be removed to an acceptable level of less than 5 ppm before the polymerization process.<sup>2-4</sup> If not removed, acetylene impurities impact the life span of the polymerizing catalyst and the quality of the polymeric products. To purify streams from acetylene, highly active catalysts are needed to selectively hydrogenate acetylene to ethylene. As shown in **Figure 1**, a selective catalyst converts acetylene to ethylene without forming ethane through ethylene over-hydrogenation or converting acetylene to oligomers.

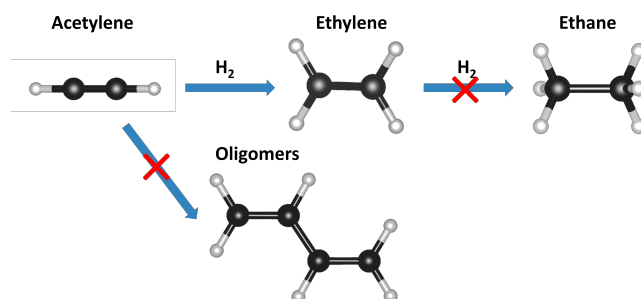


**Figure 1.** Possible products during acetylene hydrogenation reaction: ethylene (desired), ethane (undesired) or 1,3-butadiene, and other oligomers (undesired).

Intermetallic catalysts have been the subject of intensive research interest recently.<sup>5-7</sup> An intermetallic is a phase of a binary system where atoms are in an ordered arrangement, and they offer several advantages over disordered alloys. For example, when evaluating the catalytic performance of the Pd-Cu catalyst in the ordered and disordered phases, a 40% increase in ethylene selectivity was obtained when Pd and Cu atoms were in an ordered arrangement due to the improved surface dispersion.<sup>8</sup> Moreover, intermetallics are known to exhibit high thermodynamic stability and less risk of surface segregation.<sup>9-12</sup> Surface segregation presents a major drawback in the highly industrially utilized Pd-Ag alloys, where Pd islands create an ideal environment for acetylene oligomerization.<sup>13</sup>

Intermetallics are also distinct from Single Atom Alloys (SAAs), which are limited to mononuclear assemblies and require low surface densities for site isolation. In contrast,

intermetallics offer more control over the ensemble of active sites and consistent site isolation with a high density of active sites on the surface.<sup>9,14-16</sup> Most importantly, the controlled composition of intermetallics allows for a direct comparison with theoretical predictions, making them suitable and practical model catalysts.<sup>14</sup>

Pd and Pt based catalysts have been used for decades for hydrocarbon hydrogenation.<sup>2,17</sup> The promotion effect of In on Pd catalysts was studied experimentally and theoretically by Cao *et al.* and Luo *et al.*<sup>12,18</sup> The Pd-In intermetallic catalyst showed a remarkable activity and selectivity improvement in the acetylene hydrogenation reaction in comparison to the monometallic Pd catalyst, as well as high stability under reaction conditions.<sup>12</sup> The intermetallic compound also suppressed the formation of palladium hydrides, which were precursors to producing ethane.<sup>12,19</sup> However, the cost and the scarcity of these metals motivate the need to find economical and noble metal-free alternatives.

Ni was identified as a promising low-cost and abundant replacement. However, its utilization as a catalyst was limited due to its low selectivity and susceptibility to produce high levels of ethane and oligomers, mainly attributed to its strong adsorption of acetylene and ethylene relative to hydrogen.<sup>20,21</sup> Therefore, it is important to reduce the adsorption strength of acetylene and ethylene to suppress oligomerization and enhance ethylene selectivity. To do this, a second metal can be added to modify the electronic properties and reduce the adsorption energy of molecules.<sup>18,22-24</sup>

To accelerate the discovery of a selective Ni-based catalyst, many screening descriptors were proposed in the literature focusing on the formation of ethylene versus ethane as the sole factor in determining selectivity.<sup>14,17,25-28</sup> A wide computational screening of bimetallic catalysts was reported by Studt *et al.*<sup>26</sup> where NiZn was identified as a selective catalyst based on the low levels of ethane production. Later on, a study done by Spanjers *et al.*<sup>20</sup> proved that ethane production was an inaccurate descriptor for ethylene selectivity when the facile formation of oligomers was neglected. Also, despite the fact that NiZn was more selective to ethylene than monometallic Ni during experimental testing, the DFT-based energy diagrams were indicating otherwise.<sup>20</sup> This could be ascribed to discounting the coverage effect in DFT calculations, meaning that adsorption energies and activation barriers were assumed to be coverage independent and were evaluated at low coverage. Thus, the impact of adsorbate-adsorbate interactions on the surface was not considered. This assumption may cause disagreement between experimental and theoretical studies and mispredict the selectivity of catalysts, which introduces the need to study the coverage

effect in microkinetic models to reconcile theoretical calculations with experimental observations and provide more accurate insights.

Inconsistencies in the literature may also arise from using a pure acetylene and hydrogen feed when screening catalysts,<sup>29,30</sup> which is not representative of the ethylene-rich feed utilized in industrial settings. Isotopic labeling of acetylene and ethylene showed that ethane was mainly produced through the hydrogenation of the ethylene in the feed.<sup>20</sup> Thus, testing catalysts with pure acetylene may give the wrong impression about the selectivity of catalysts under real reaction conditions.

Even though acetylene hydrogenation reactions were studied extensively both experimentally and theoretically, there is still a lack of understanding of the reaction kinetics on the emerging intermetallic Ni-based catalysts. In this work, we present DFT-based modeling of Ni, together with Ni<sub>3</sub>In, NiIn, and Ni<sub>2</sub>In<sub>3</sub> intermetallics to describe the key hydrogenation and oligomerization reactions of acetylene. We show that the formation of the Ni-In intermetallic compounds may result in favorable geometric and electronic effects that can tune the hydrogenation activity and potentially enhance the selectivity for ethylene. The Ni-In phase diagram in **Figure S1** shows that Ni<sub>3</sub>In, NiIn, and Ni<sub>2</sub>In<sub>3</sub> all exist as an intermetallic phase.<sup>31</sup> The selected formulations have a reasonable bulk unit cell size for computation (**Table S1-S3**) and available synthesis recipes in the literature.<sup>23,32</sup> Additionally, these formulations exhibit a range of low, intermediate, and high In incorporation on Ni surfaces allowing us to understand trends. We studied the promotional effect of introducing In to metallic Ni against a monometallic Ni surface. We constructed reaction profiles at low and high coverage of acetylene based on the elementary steps of the hydrogenation and oligomerization reactions and addressed the competition between them when evaluating the selectivity of the catalysts. We also developed a microkinetic model to predict the activity and the selectivity of the catalysts under reaction conditions and investigated the impact of feed composition. Our study aims to unravel the promotional effect of In on Ni-based intermetallic catalysts while considering oligomerization reactions, coverage effect, and feed composition. We highlight the importance of accounting for these factors to develop a comprehensive understanding of the catalytic selectivity in acetylene hydrogenation reactions.

## 2. METHODS

### 2.1 Density Functional Theory (DFT) Methods

All DFT calculations were performed using the Vienna Ab-initio Simulation Package (VASP).<sup>33,34</sup> The interaction between the ionic core and the valence electrons was described by the projector-augmented wave (PAW) method.<sup>35,36</sup> The valence one electron functions were developed on a basis set of planes waves with an energy cutoff of 400 eV. The Perdew–Burke–Ernzerhof (PBE) exchange-correlation functional in the framework of the generalized gradient approximation (GGA)<sup>37</sup> was employed to calculate the electronic structures. Dispersion interactions were included using the DFT-D3 method of Grimme.<sup>38,39</sup> The force convergence threshold was set to 0.03 eV/Å and spin polarization was considered. Surfaces were modeled by 4×4 supercells<sup>27,28</sup> and four-atomic-layer slabs. The two topmost layers and adsorbates were relaxed, and the rest of the layers were fixed to bulk composition except when calculating surface energies.

Sampling of the Brillouin zone was performed by 3×3×1 Gamma-centered **k**-point mesh for NiIn and Ni<sub>2</sub>In<sub>3</sub>. 4×4×1 and 5×5×1 Gamma-centered **k**-point mesh were used for Ni<sub>3</sub>In and Ni surfaces, respectively. **K**-point mesh sizes were scaled based on bulk unit cell optimization. Each slab was separated from the next one in the z-direction by a vacuum of 15 Å to eliminate the interaction between them.

To determine the most exposed facet during the hydrogenation reaction, surface energies of the low-index facets for Ni<sub>3</sub>In (Table S4) and Ni<sub>2</sub>In<sub>3</sub> (Table S5) were calculated using equation 1.

$$\gamma = \frac{(E_{\text{slab}} - NE_{\text{bulk}})}{2A} \quad (1)$$

where  $E_{\text{slab}}$  is the total energy of the clean slab,  $N$  is the number of equivalent bulk unit cells for the slab and  $E_{\text{bulk}}$  is the energy of a single bulk unit cell.  $A$  is the area of the slab multiplied by a factor of two to account for the top and bottom surface area. This equation assumes that the top and bottom surfaces are equivalent and that the slab is stoichiometric.

Possible adsorption sites for reactants, intermediates, and products were explored on Ni<sub>3</sub>In (Table S6), NiIn (Table S7), and Ni<sub>2</sub>In<sub>3</sub> (Table S8). The adsorption energy of the gaseous molecules was calculated following equation 2.

$$\Delta E_{\text{adsorption}} = E_{\text{adsorbate/surface}} - E_{\text{surface}} - E_{\text{adsorbate}} \quad (2)$$

where  $\Delta E_{\text{adsorption}}$  is the adsorption energy,  $E_{\text{adsorbate/surface}}$  is the total energy of the gaseous molecule adsorbed on the surface of the slab,  $E_{\text{surface}}$  is the energy of the clean slab surface and  $E_{\text{adsorbate}}$  is the energy of the gaseous molecule. Adsorption sites for Ni are studied in the literature.<sup>20,24,40,41</sup>

The Gibbs free energy for acetylene hydrogenation and oligomerization reactions was calculated according to [equation 3](#) while treating all vibrational degrees of freedom harmonically.

$$G = E + E_{\text{vib}} + PV - T \times S \quad (3)$$

where G is Gibb's free energy, E and  $E_{\text{vib}}$  are the internal energy and vibrational energy of the system. The contribution of pressure and volume (PV) is assumed to be negligible.<sup>24,42</sup> T is the reaction temperature (433 K) and S is the entropy.

The vibration analysis package in the Atomic Simulation Environment (ASE)<sup>43</sup> was used to calculate  $E_{\text{vib}}$  and vibrational entropy. All atoms were frozen except adsorbates. Transition states (TS) were calculated using the climbing image-nudged elastic band (CI-NEB) method with 8 images.<sup>44</sup> CI-NEB calculations were subsequently converged by the Quasi-Newton method or the dimer method by Henkelman *et al.*<sup>45</sup> Vibrational frequency calculations were also used to verify transition states, resulting in a single imaginary frequency along the reaction coordinate.

## 2.2 Microkinetic Model

The microkinetic model was constructed based on the nine elementary steps presented in [Table 1](#) with no assumption of a rate-determining step. The system of ordinary differential equations resulting from the elementary steps and the calculated reaction constants was solved in MATLAB (version R2022b) using an in-build solver "ode15s", which is fit for solving a set of stiff differential equations.<sup>46</sup>

One monolayer coverage of  $\text{C}_2\text{H}_2$  on Ni, NiIn, and  $\text{Ni}_3\text{In}$  was assumed to be 8  $\text{C}_2\text{H}_2$  molecules (one  $\text{C}_2\text{H}_2$  molecule for two surface metal atoms) and 10  $\text{C}_2\text{H}_2$  molecules for  $\text{Ni}_2\text{In}_3$  because the surface unit cell for  $\text{Ni}_2\text{In}_3$  is larger. For H atom, one monolayer coverage was assumed to be 16 H atoms on Ni, NiIn, and  $\text{Ni}_3\text{In}$  and 20 H atoms on  $\text{Ni}_2\text{In}_3$ . For the high coverage model, a single type of adsorbate, in this case,  $\text{C}_2\text{H}_2$ , was used to simulate all the adsorbate-adsorbate interactions

in the systems. C<sub>2</sub>H<sub>2</sub> was selected as the high coverage environmental species because the microkinetic model showed that it was the most abundant surface intermediate. It was also proven that using C<sub>2</sub>H<sub>2</sub> to describe the multi-adsorbate systems for this reaction was appropriate because C<sub>2</sub>H<sub>2</sub> and C<sub>2</sub>H<sub>4</sub> showed similar self and cross-interactions.<sup>27</sup>

The low coverage kinetic simulations used free energy profiles calculated on bare surfaces, with one acetylene and one H atom on the considered 4x4 unit cell, and the initial condition for the kinetics was a bare surface. In contrast, the high coverage simulations used free energy profiles calculated with 0.5 ML of acetylene for Ni, Ni<sub>3</sub>In, and NiIn and 0.6 ML for Ni<sub>2</sub>In<sub>3</sub>, as justified later. Hence, the coverage of available empty sites was 0.5 ML (0.4 ML respectively). An additional acetylene molecule was adsorbed, together with two H atoms and the free energy pathways correspond to the reaction of that additional acetylene molecule. These pathways show differential adsorption and reaction free energies with reference to a surface pre-covered by 0.5 ML (or 0.6 ML) of acetylene, and these differential reaction energies were used for the kinetic simulations. Higher coverage of environmental acetylene was used for Ni<sub>2</sub>In<sub>3</sub> because it was significantly more stable than the 0.5 ML case (Figure S2 (c)), allowing the reaction to take place between 0.6 ML and 0.7 ML, which were the most stable coverages. Kinetic simulations at high coverage were initiated with a total coverage of C<sub>2</sub>H<sub>2</sub> (environmental + reacting) of 0.75 ML for Ni, NiIn, and Ni<sub>3</sub>In and 0.8 ML for Ni<sub>2</sub>In<sub>3</sub>.

For the surface reaction steps, the rate constants were calculated according to the conventional transition state theory in equation 4.

$$k_i = \frac{k_B T}{h} e^{-\Delta G_i^\ddagger / k_B T} \quad (4)$$

where  $k_B$  is the Boltzmann constant,  $T$  is the reaction temperature,  $h$  is the Planck's constant and  $\Delta G_i^\ddagger$  the change of standard molar Gibbs free energies between the TS and the initial state for step  $i$ , where  $i = 1, \dots, 9$ .

For the adsorption steps, the rate constants were assumed to be non-activated and were limited to the flux of molecules to the surface according to equation 5 and following the kinetic theory of gases.

$$k_{\text{adsorption}} = \frac{\sigma P^0 A}{\sqrt{2\pi m k_B T}} \quad (5)$$



Where  $\sigma$  is the initial sticking probability taken here as 1,  $P^\circ$  is the standard pressure and  $m$  is the mass of the adsorbate.  $A$  is the surface area for one active site, a typical value of  $10^{-19} \text{ m}^2$  was used here.<sup>47,48</sup> For the desorption steps, rate constants were calculated from the adsorption equilibrium,  $K_{\text{adsorption}}$  and the rate constant for adsorption ensuring thermodynamic consistency as shown in **equation 6**. All  $k$  values were expressed in  $\text{s}^{-1}$ .

$$k_{\text{desorption}} = \frac{k_{\text{adsorption}}}{K_{\text{adsorption}}} \quad (6)$$

The microkinetic model was embedded in a batch reactor model<sup>20</sup> to provide a more realistic and accurate representation of the reaction system and enable the prediction of key performance indicators such as conversion, selectivity, and yield. To mimic the industrial feed composition, a total pressure of  $\sim 10$  bar and a partial pressure ratio of 1:1:100  $\text{C}_2\text{H}_2:\text{H}_2:\text{C}_2\text{H}_4$  was employed. All kinetic and thermodynamic calculations were done at a reaction temperature of 433 K to reflect the experimental conditions.<sup>20</sup>

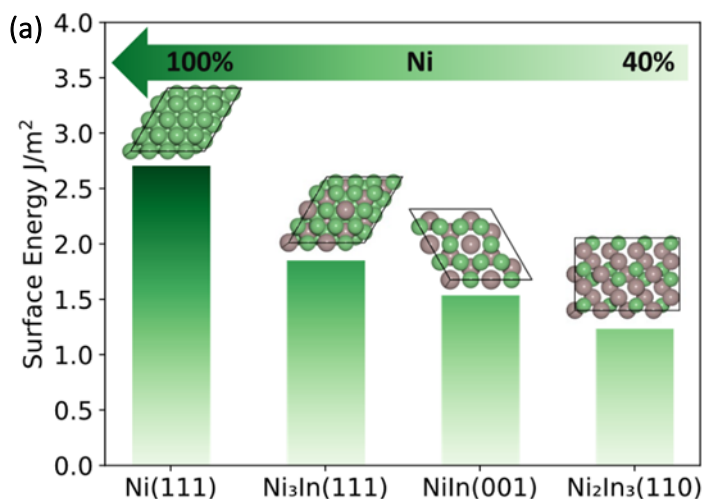
**Table 1.** Elementary steps and rate equations of acetylene hydrogenation and oligomerization reactions used in the microkinetic modeling (\* represents the free site on the surface)

surface reaction	rate equation
1 $\text{C}_2\text{H}_2(\text{g}) + * \leftrightarrow \text{C}_2\text{H}_2^*$	$r_1 = k_1\theta_*P_{\text{C}_2\text{H}_2} / P^\circ - k_{-1}\theta_{\text{C}_2\text{H}_2}$
2 $\text{H}_2(\text{g}) + 2* \leftrightarrow 2\text{H}^*$	$r_2 = k_2\theta_*^2P_{\text{H}_2} / P^\circ - k_{-2}\theta_{\text{H}}^2$
3 $\text{C}_2\text{H}_2^* + \text{H}^* \leftrightarrow \text{C}_2\text{H}_3^* + *$	$r_3 = k_3\theta_{\text{C}_2\text{H}_2}\theta_{\text{H}} - k_{-3}\theta_{\text{C}_2\text{H}_3}\theta_*$
4 $\text{C}_2\text{H}_3^* + \text{H}^* \leftrightarrow \text{C}_2\text{H}_4^* + *$	$r_4 = k_4\theta_{\text{C}_2\text{H}_3}\theta_{\text{H}} - k_{-4}\theta_{\text{C}_2\text{H}_4}\theta_*$
5 $\text{C}_2\text{H}_4^* \leftrightarrow \text{C}_2\text{H}_4(\text{g}) + *$	$r_5 = k_5\theta_{\text{C}_2\text{H}_4} - k_{-5}\theta_*P_{\text{C}_2\text{H}_4} / P^\circ$
6 $\text{C}_2\text{H}_4^* + \text{H}^* \leftrightarrow \text{C}_2\text{H}_5^* + *$	$r_6 = k_6\theta_{\text{C}_2\text{H}_4}\theta_{\text{H}} - k_{-6}\theta_{\text{C}_2\text{H}_5}\theta_*$
7 $\text{C}_2\text{H}_5^* + \text{H}^* \leftrightarrow \text{C}_2\text{H}_6(\text{g}) + 2*$	$r_7 = k_7\theta_{\text{C}_2\text{H}_5}\theta_{\text{H}} - k_{-7}\theta_*^2P_{\text{C}_2\text{H}_6} / P^\circ$
8 $\text{C}_2\text{H}_2^* + \text{C}_2\text{H}_3^* \leftrightarrow \text{C}_4\text{H}_5^* + *$	$r_8 = k_8\theta_{\text{C}_2\text{H}_2}\theta_{\text{C}_2\text{H}_3} - k_{-8}\theta_{\text{C}_4\text{H}_5}$
9 $\text{C}_4\text{H}_5^* + \text{H}^* \leftrightarrow \text{C}_4\text{H}_6(\text{g}) + 2*$	$r_9 = k_9\theta_{\text{C}_4\text{H}_5}\theta_{\text{H}} - k_{-9}\theta_*^2P_{\text{C}_4\text{H}_6} / P^\circ$

### 3. RESULTS AND DISCUSSION

#### 3.1 Surface Energy and Adsorption Sites

The surface energy of low-index facets of Ni, Ni<sub>3</sub>In, NiIn, and Ni<sub>2</sub>In<sub>3</sub> was calculated to determine the most stable and energetically favorable facet for each material. Symmetry on the Ni<sub>3</sub>In surface reduced the number of studied surfaces to three facets only (Table S4), while Ni<sub>2</sub>In<sub>3</sub> had a less symmetric nature with five distinguished facets (Table S5). For NiIn, the (001) facet was selected according to the study by Song *et al.*<sup>24</sup> Ni (111) was selected because it is the most energetically favorable facet<sup>49</sup> and was extensively studied in the literature, particularly in the contexts of acetylene hydrogenation reactions.<sup>5,20,24,40</sup> The as-cut composition was preserved for all the facets. The most stable facets were Ni<sub>3</sub>In (111), NiIn (001), and Ni<sub>2</sub>In<sub>3</sub> (110) and these facets are assumed when referring to these surfaces for the rest of this work. As shown in Figure 2 (a), the lowest surface energy among all the explored surfaces was for Ni<sub>2</sub>In<sub>3</sub> (110) with 1.23 J/m<sup>2</sup> and the largest surface energy was for Ni (111) with 2.71 J/m<sup>2</sup>. Overall, surface energies were increasing with increasing the Ni content of the surface. These findings may have important implications for understanding the behavior of these surfaces during chemical reactions.



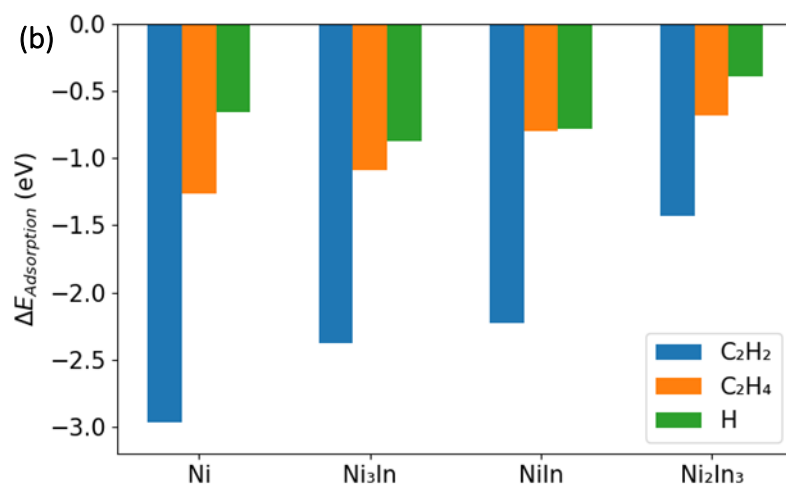


**Figure 2.** (a) Surface energies ( $\text{J/m}^2$ ) of the most stable low-index facets of Ni, Ni<sub>3</sub>In, NiIn, and Ni<sub>2</sub>In<sub>3</sub>. Color coding: Ni (green) and In (brown). Surface energies were increasing with increasing the Ni content of the surface. (b) Adsorption energies (eV) of C<sub>2</sub>H<sub>2</sub>, C<sub>2</sub>H<sub>4</sub>, and H at low coverage (only one species adsorbed on the unit cell). Adsorption energies of acetylene and ethylene were increasing with increasing the Ni content of the surface.

The shortest Ni-Ni distances, the corresponding Ni-Ni coordination numbers and d-band centers ( $\epsilon_d$ ) for Ni (111), Ni<sub>3</sub>In (111), NiIn (001), and Ni<sub>2</sub>In<sub>3</sub> (110) were calculated to understand the structural and electronic properties of these surfaces and are presented in Table 2. The Geometric effect caused by the isolation of Ni active sites is demonstrated by the shortest Ni-Ni distance on the surfaces as well as the Ni-Ni coordination numbers. The Ni-Ni coordination number was determined by counting the nearest neighbors of Ni atoms. Table 2 shows that Ni<sub>2</sub>In<sub>3</sub> (110) exhibited complete isolation of the Ni active sites while Ni<sub>3</sub>In (111) and NiIn (001) exhibited partial isolation. Modifications on the electronic structures of the 3d orbital of Ni are shown by the Density of States (DOS) calculations (Figure S4). The electronic properties of Ni are significantly modified upon the formation of intermetallic compounds, resulting in narrower d-bands and higher d-band centers when the In content on the surface increases.

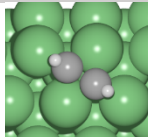
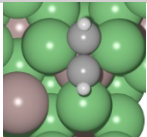
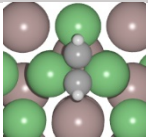
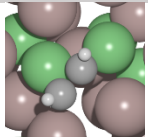
**Table 2.** Shortest Ni-Ni distances (Å), Ni-Ni coordination number, and d-band centers ( $\epsilon_d$ ) with respect to the Fermi level of Ni 3d orbitals on Ni (111), Ni<sub>3</sub>In (111), NiIn (001), and Ni<sub>2</sub>In<sub>3</sub> (110).

surface	shortest Ni-Ni distance (Å)	Ni-Ni coordination number	$\epsilon_d$
Ni (111)	2.45	9	-1.66
Ni <sub>3</sub> In (111)	2.50	6	-1.29
NiIn (001)	2.61	4	-1.36
Ni <sub>2</sub> In <sub>3</sub> (110)	2.87	2 <sup>a</sup>	-1.10

<sup>a</sup> one Ni atom was at distance of 2.93 Å.

The evaluation of the possible adsorption sites on the most stable facets (Table S6-S8) revealed that In atoms were less active than Ni atoms. The most stable acetylene configurations on all the surfaces are shown in Table 3. Acetylene was always adsorbed on the Ni atoms or bridging with In atoms at high In content surfaces. The bond distances (also shown in Table 3) refer to the nearest Ni or In atom to a carbon atom in the acetylene molecule. The large distances between In and C atoms on Ni<sub>3</sub>In, NiIn, and Ni<sub>2</sub>In<sub>3</sub> indicate the lack of bonding between acetylene and In atoms thus, proves their lower catalytic activity compared to Ni. The overall weak adsorption energies and the low activity of In atoms came in agreement with the previous computational and experimental findings.<sup>24,30</sup>

**Table 3.** Most stable configurations, low coverage adsorption energies (eV) and corresponding bond distances (Å) for acetylene. Color coding: Ni (green), In (brown), H (white), and C (gray). The large distances between In and C atoms indicate the low catalytic activity of In.

	Ni	Ni <sub>3</sub> In	NiIn	Ni <sub>2</sub> In <sub>3</sub>
acetylene configuration				
$\Delta E_{\text{ads}}$	-2.97	-2.38	-2.23	-1.43
C-Ni bond (Å)	2.01	2.10	2.00	1.99
C-In bond (Å)	-	3.51	2.42	2.28

Low coverage adsorption energies of acetylene, ethylene, and hydrogen on the most stable facets are presented in **Figure 2 (b)**. Results show that the adsorption energy of acetylene decreases as the surface composition changes from Ni to Ni<sub>2</sub>In<sub>3</sub>, with the strongest adsorption energy value of -2.97 eV observed on Ni and the weakest adsorption energy value of -1.43 eV observed on Ni<sub>2</sub>In<sub>3</sub>. This could be caused by the Ni ensemble effect. Acetylene adsorbs on 4 Ni atoms on Ni, but it can only interact with Ni<sub>3</sub> ensembles on Ni<sub>3</sub>In and NiIn, and with Ni<sub>2</sub> ensembles for Ni<sub>2</sub>In<sub>3</sub>. However, the difference in the adsorption energy of acetylene between Ni<sub>3</sub>In and NiIn was small (0.15 eV) as they exhibit a similar Ni ensemble.

Notably, the hydrogen adsorption energy on Ni<sub>3</sub>In and NiIn was slightly stronger than the hydrogen adsorption energy on Ni. Furthermore, the adsorption energy of hydrogen and ethylene was found to become similar on NiIn. The change in adsorption energies with surface composition was less pronounced in the case of ethylene in comparison to acetylene, but both followed the same trend and became stronger with increasing the Ni content of the surfaces, in line with the increase of the accessible Ni ensemble size for acetylene. Previous theoretical and experimental research has established the presence of strong electron interactions between Ni and In in Ni-In intermetallic compounds. Electron transfer from the electropositive In atoms to the Ni atoms was evidenced in electron density contour maps.<sup>22,23,50</sup> Thus, the charge transfer from In to Ni and the active-site isolation of Ni in Ni-In intermetallics resulted in reduced adsorption strength of acetylene and ethylene in comparison to Ni.

### 3.2 Low Coverage Acetylene Reaction Profiles

Reaction profiles with low coverage of reactants, acetylene and hydrogen, were calculated to provide insights about the adsorption properties and activation barriers of individual molecules or atoms on the surface. The first step in the hydrogenation pathway is the C-H bond formation on the adsorbed acetylene molecule producing vinyl. Vinyl is then further hydrogenated to form ethylene. Ethylene will either desorb from the surface or over-hydrogenate and form ethane. Similarly, ethylene in the reaction feed can adsorb on the catalyst and be hydrogenated, which is undesirable. A selective catalyst should have a small ethylene desorption energy and a high ethylene hydrogenation barrier to avoid over-hydrogenation. The hydrogenation reaction profile is shown in **Figure 3**. The reaction profiles start with acetylene adsorption on the surface and follow the Horiuti–Polanyi mechanism.<sup>35</sup> In the Horiuti–Polanyi mechanism, the acetylene is being sequentially hydrogenated by the addition of atomic H.<sup>5</sup> The adsorption energy of acetylene is weakened with the presence of In on the surface with Ni<sub>2</sub>In<sub>3</sub> exhibiting the lowest binding energy. The first two activation energies in the reaction profile control the activity of the surface.<sup>28</sup> NiIn exhibits the highest acetylene hydrogenation barrier (1.00 eV), while the energy barriers for the other surfaces range from 0.82-0.84 eV (**Table S9**). Surfaces also show comparable second hydrogenation barriers except for Ni<sub>2</sub>In<sub>3</sub> (**Table S9**); Ni<sub>2</sub>In<sub>3</sub> has a high energy barrier for vinyl hydrogenation (1.12 eV), which poses a challenge for the hydrogenation reaction to proceed.

The calculated values of energy barriers of ethylene hydrogenation and ethylene desorption energy are presented in **Table 4**. Ethylene hydrogenation barriers and ethylene desorption energies are both decreased in the Ni-In surfaces in comparison to Ni. The enhanced ethylene desorption on Ni-In catalysts could be ascribed to the Ni site-isolation effect (**Table 2**), which is one of the advantageous characteristics of intermetallic compounds. This is because extended active sites are typically responsible for the strong adsorption of unsaturated hydrocarbons which subsequently catalyze undesired reactions.<sup>2,20,51</sup> The Gibbs free energy difference ( $\Delta G$ ) between the ethylene hydrogenation barrier ( $\Delta G_{TS}$ ) and ethylene desorption energy ( $\Delta G_{des}$ ) has been used as a descriptor for ethylene selectivity in previous studies.<sup>17,52,53</sup> A higher  $\Delta G$  value is expected to indicate a greater preference for the formation of ethylene. However, further investigation showed that this descriptor was inaccurate as the microkinetic model revealed that Ni<sub>3</sub>In had the highest ethylene yield despite having the lowest  $\Delta G$  value, as discussed later.

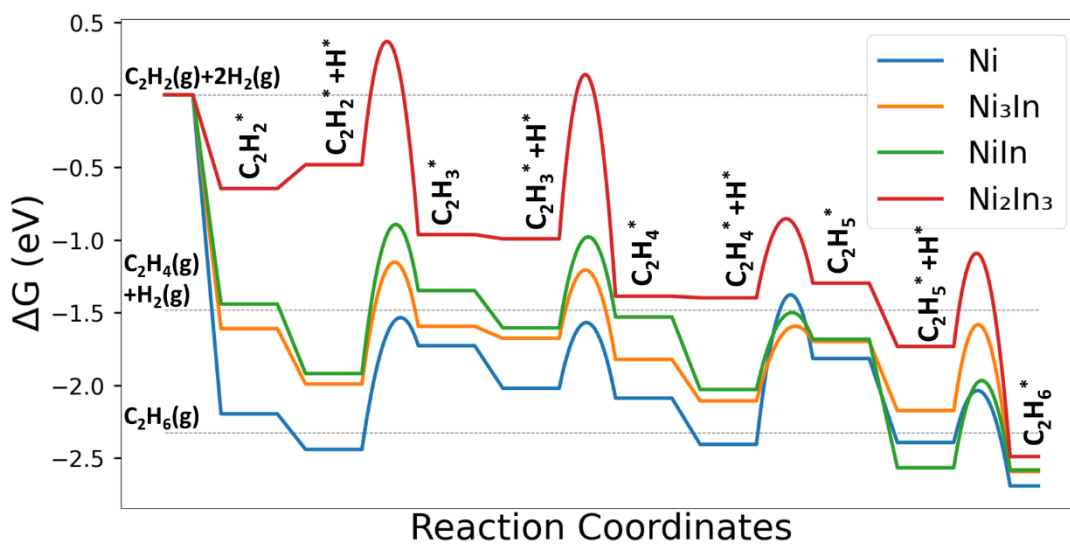


**Figure 3.** Gibbs free energy profiles of acetylene hydrogenation on Ni, Ni<sub>3</sub>In, NiIn, and Ni<sub>2</sub>In<sub>3</sub> at 433 K at low coverage. Energies are relative to bare surface, C<sub>2</sub>H<sub>2</sub>(g) and 2H<sub>2</sub>(g) (dotted line). The gas phase reaction energy to form C<sub>2</sub>H<sub>4</sub> and C<sub>2</sub>H<sub>6</sub> is indicated with thin dotted lines. The reaction profiles follow the Horiuti-Polanyi mechanism where acetylene is sequentially hydrogenated by atomic H.

**Table 4.** Ethylene over hydrogenation barrier  $\Delta G_{TS}$  (eV) (elementary step 6 in Table 1), desorption energy  $\Delta G_{des}$  (eV) (elementary step 5 in Table 1), and the difference between the two values ( $\Delta G$ ). ( $\Delta G$ ) was proposed as a selectivity descriptor in previous studies,<sup>17,52,53</sup> where a higher  $\Delta G$  value is expected to indicate a greater selectivity to ethylene.

$\Delta G$ eV	Ni	Ni <sub>3</sub> In	NiIn	Ni <sub>2</sub> In <sub>3</sub>
over hydrogenation barrier $\Delta G_{TS}$	1.00	0.48	0.51	0.54
desorption $\Delta G_{des}$	0.62	0.34	0.05	-0.09
$\Delta G = \Delta G_{TS} - \Delta G_{des}$	0.38	0.14	0.46	0.54

The formation of C<sub>4</sub> hydrocarbon oligomers through C-C coupling is a key step in determining the overall selectivity of the catalysts, as it competes with the hydrogenation of acetylene and the formation of ethylene. Figure 4 shows the reaction profiles of C-C bond formation between

adsorbed acetylene and vinyl. The proposed mechanism starts with the adsorption of an acetylene molecule, followed by the addition of a hydrogen atom to form vinyl. Next, a carbon-carbon bond is formed between vinyl and another adsorbed acetylene molecule, and the final step is the hydrogenation of  $C_4H_5$  to produce butadiene. While there are other possible reactions for C-C coupling between molecules such as acetylene, vinylidene, and vinyl, the literature agrees that the most kinetically favorable precursors for oligomers were acetylene and vinyl.<sup>20</sup>

In comparison to Pd surfaces, on which C4 hydrocarbon was stabilized by four Pd atoms,<sup>54</sup>  $Ni_2In_3$  showed C4 hydrocarbon stability with only two isolated Ni atoms as shown in Figure S5. The smallest C-C coupling barrier was observed on NiIn (0.75 eV), which also exhibited the largest acetylene hydrogenation barrier (1.00 eV) (Table S9). Thus, acetylene seems more likely to oligomerize than to hydrogenate over NiIn. The complexity of the reaction network and the different parameters that contributed to the selectivity of the catalysts introduce the need for microkinetic modeling to provide more insights, as discussed later.

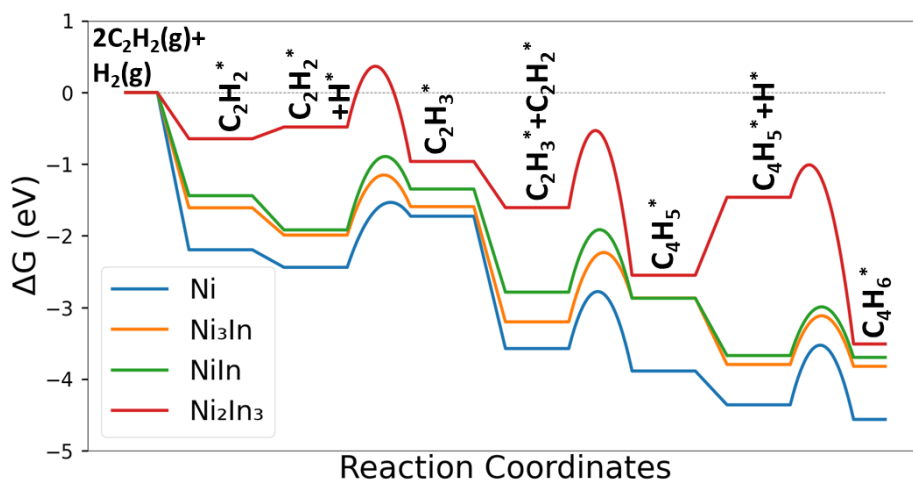


**Figure 4.** Gibbs free energy profiles of acetylene oligomerization on Ni,  $Ni_3In$ , NiIn, and  $Ni_2In_3$  at 433 K at low coverage. Energies are relative to bare surface,  $2C_2H_2(g)$  and  $H_2(g)$  (dotted line). The reaction starts with the hydrogenation of adsorbed acetylene molecule to form  $C_2H_3$  followed by a C-C bond formation between  $C_2H_3$  and another adsorbed acetylene. The last step is  $C_4H_5$  hydrogenation to form butadiene.



### 3.3 Coverage-Dependent Binding Energies

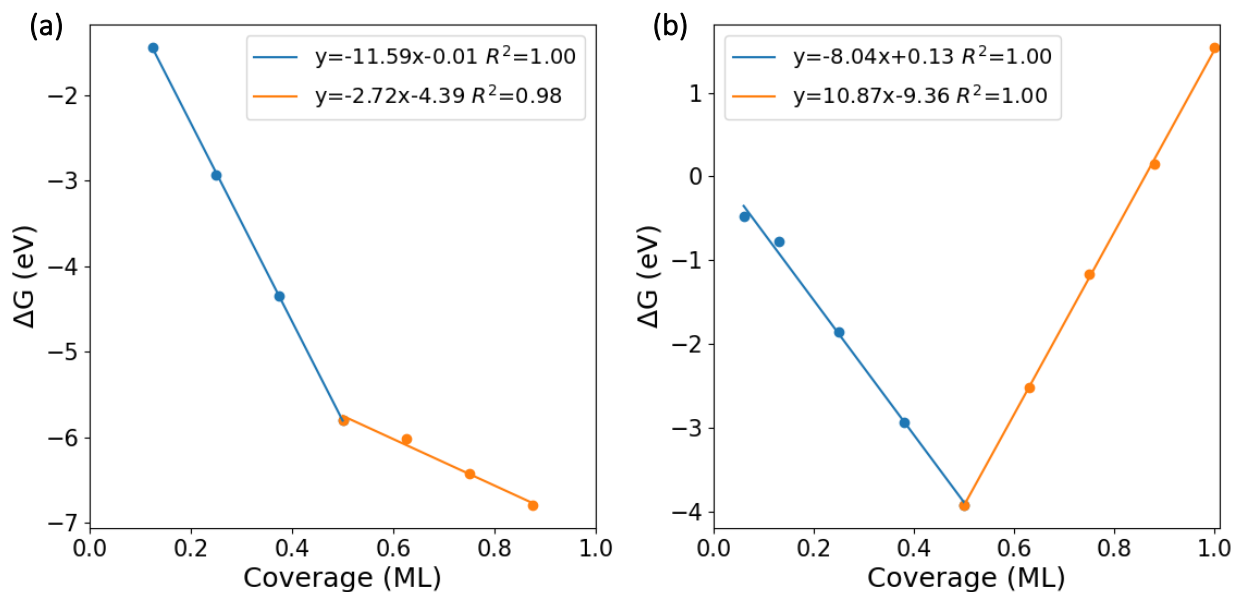
To accurately describe the surface species population under reaction conditions, it is important to understand how the adsorption energy changes with the coverage of adsorbates. It was found from previous studies<sup>27,28,55</sup> that the coverage-dependent behavior of adsorption energies was only apparent when a specific coverage threshold was reached.

The exploration of high coverage situations was done by manually generating initial configurations. Surveying the adsorption sites at low coverage provided an idea about the stability of each site e.g. molecules do not adsorb at the top of In atom. Also, the symmetry of the surface may reduce the possible configurations as some adsorption sites can be equivalent. Resulting configuration geometries and energies for Ni, Ni<sub>3</sub>In, NiIn and Ni<sub>2</sub>In<sub>3</sub> for acetylene coverages of 0.5, 0.625/0.6 and 0.75/0.7 ML are shown in [Tables S10-S13](#).

The average adsorption free energies of acetylene as a function of coverage are shown in [Figure S3](#) to allow for a better comparison with experimental data. Here, NiIn was selected as a model system to investigate the change in binding energies with respect to coverage, while other systems can be found in [Figure S2](#). Initially, the total adsorption free energy of acetylene on a 4×4 slab of NiIn increases in absolute value linearly with increasing coverage ([Figure 5 \(a\)](#)). However, once the threshold coverage ( $\Theta=0.5$  ML) was surpassed, the total adsorption free energy for C<sub>2</sub>H<sub>2</sub> was weakened as indicated by the reduced slope of the linear fit. [Figure 5 \(a\)](#) does not include data for a C<sub>2</sub>H<sub>2</sub> coverage of 1 ML, as the aggregation of the C<sub>2</sub>H<sub>2</sub> molecules on the surface caused oligomerization after the placement of 8 C<sub>2</sub>H<sub>2</sub> molecules in the unit cell ([Figure S6](#)). A similar two-slope behavior was found for H adsorption free energy versus coverage, with the same threshold coverage ( $\Theta=0.5$  ML). However, the total adsorption free energy for H becomes positive (destabilizing) after this threshold ([Figure 5 \(b\)](#)).

The decrease in adsorption free energy after the threshold coverage varied in its extent between C<sub>2</sub>H<sub>2</sub> and H due to the different properties of these molecules. This is because all the favorable adsorption sites for H were occupied at 0.5 ML coverage ([Figure S7](#)). As a result, the added hydrogen atoms resided on less stable sites when the coverage was above the threshold. H atoms in general exhibit negligible repulsive interactions with themselves and other adsorbates due to

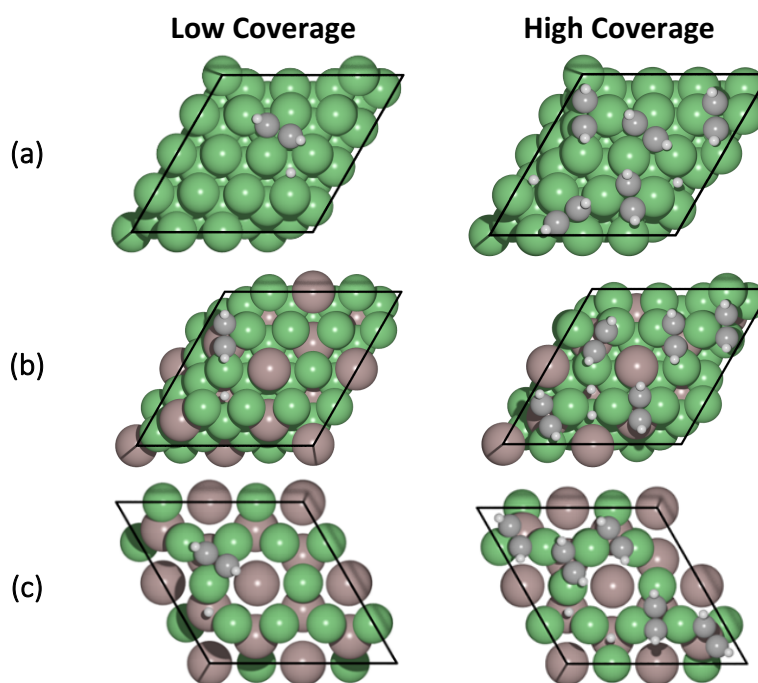
their small size which deemed them unsuitable to describe the coverage effect on reaction at surfaces.<sup>5,55,56</sup>



**Figure 5.** Total chemisorption free energies at 433 K versus coverage of (a)  $C_2H_2$  and (b) H on a  $4 \times 4$  supercell of NiIn. Data for a  $C_2H_2$  coverage of 1 ML is not shown because the aggregation of the  $C_2H_2$  molecules on the surface caused oligomerization. Low coverage data points and linear fit are shown by the blue line. High coverage data points and linear fit are shown by the orange line. In both cases, adsorption of  $C_2H_2$  and H is weakened after a threshold coverage of 0.5 ML.

### 3.4 Acetylene Reaction Profiles at High Coverage

Going beyond the traditional modeling simplifications is essential in determining an accurate activity and selectivity descriptor and accelerating the discovery of hydrogenation catalysts. One commonly made simplification is the assumption that the reaction is not influenced by the degree of surface coverage. In this section, all adsorption energies and energy barriers were recalculated in the presence of 0.5 ML or (0.6 ML in the case of  $\text{Ni}_2\text{In}_3$ ) initial coverage of acetylene species. The coverage of 0.5 ML is not thermodynamically the most stable for acetylene on the surfaces. It was selected because it represents the crossover between strongly bound and weakly bound molecules. Selecting 0.5 ML or (0.6 ML in the case of  $\text{Ni}_2\text{In}_3$ ) as the initial coverage for the high coverage model was also validated retrospectively through the kinetic simulations as shown in the next section. From there an additional (weakly bound) acetylene molecule was added (bringing the coverage to 0.625 ML for Ni,  $\text{Ni}_3\text{In}$ , and  $\text{NiIn}$ , and to 0.7 ML for  $\text{Ni}_2\text{In}_3$ ) and one  $\text{H}_2$  molecule was dissociated in the favorable remaining sites to construct the structures used for the hydrogenation pathway (Table S14-S15). Figure 6 presents the surface species just before the first hydrogenation step at low and high coverage.



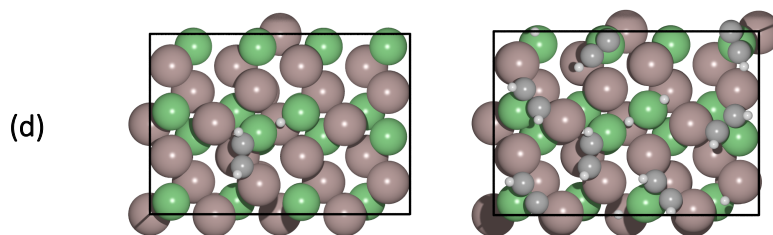


**Figure 6.** Coadsorbed acetylene and hydrogen, which is the starting configuration for the first hydrogenation step, at low (left) and high (right) acetylene coverage: (a) Ni (b) Ni<sub>3</sub>In (c) NiIn (d) Ni<sub>2</sub>In<sub>3</sub>. Color coding: Ni (green), In (brown), H (white), C (gray).

Overall, the energy barriers were reduced at high coverage for both the hydrogenation (Figure 7, Table S9) and the oligomerization pathway (Figure 8, Table S9). Significant reductions in energy barriers were observed in the first hydrogenation step and the C-C coupling step. Although the second hydrogenation energy barrier was reduced from 1.12 eV to 0.93 eV on Ni<sub>2</sub>In<sub>3</sub>, it remains relatively high, presenting a challenge for the hydrogenation reaction to continue. The reduction of energy barriers at high coverage could be explained by the fact that these are bond-forming associative reactions that decrease the number of adsorbates on the surface and, hence, lower the lateral repulsions between them.

The step with the highest local barrier along the hydrogenation pathway changes at high coverage for Ni and Ni<sub>3</sub>In. In the case of Ni, the highest local barrier shifts from the over-hydrogenation step at low coverage (Figure 3) to the first hydrogenation step at high coverage (Figure 7). In the case of Ni<sub>3</sub>In, the highest local barrier shifts from the first hydrogenation step at low coverage (Figure 3) to the second hydrogenation step at high coverage (Figure 7). For NiIn and Ni<sub>2</sub>In<sub>3</sub> the highest local barriers are the first hydrogenation step and the second hydrogenation step, respectively, regardless of the coverage.

Figure 8 shows that, at high coverage, Ni is highly prone to form oligomers, with a small C-C coupling energy barrier of 0.25 eV (Table S9). Conversely, Ni<sub>2</sub>In<sub>3</sub> has the largest C-C coupling energy barrier, with a value of 0.57 eV. However, the substantial vinyl hydrogenation energy barrier (0.93 eV) in Ni<sub>2</sub>In<sub>3</sub> is likely to steer the reaction towards oligomerization, rather than hydrogenation as was later confirmed by the microkinetic model.

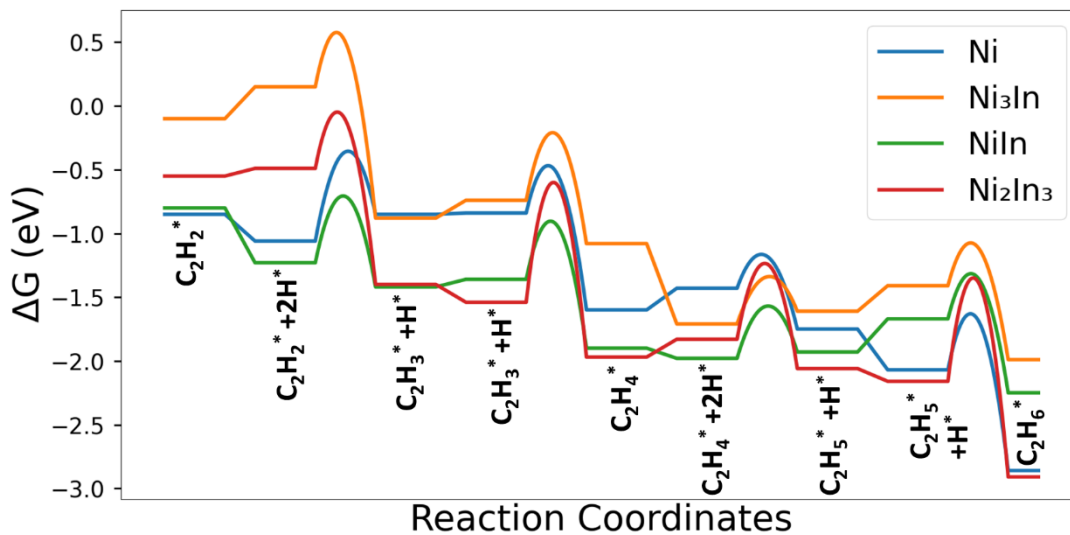


**Figure 7.** Gibbs free energy profiles of acetylene hydrogenation on Ni, Ni<sub>3</sub>In, NiIn, and Ni<sub>2</sub>In<sub>3</sub> at 433 K at high coverage. Energies are relative to surfaces with 0.5/0.6 ML of environmental C<sub>2</sub>H<sub>2</sub>. The labels assigned to each step denote the corresponding reacting species.

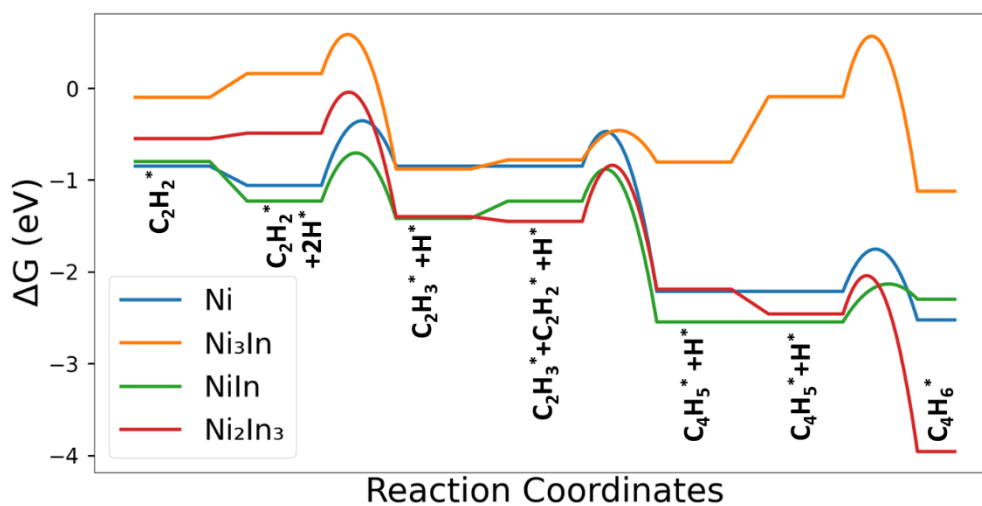


**Figure 8.** Gibbs free energy profiles of acetylene oligomerization on Ni, Ni<sub>3</sub>In, NiIn, and Ni<sub>2</sub>In<sub>3</sub> at 433 K at high coverage. Energies are relative to surfaces with 0.5/0.6 ML of environmental C<sub>2</sub>H<sub>2</sub>. The labels assigned to each step denote the corresponding reacting species.

### 3.5 Microkinetic Simulations

Kinetic modeling was then performed to study the effect of the surface reactant coverage on the activity and the selectivity of the catalysts. Species distribution for Ni<sub>3</sub>In and Ni<sub>2</sub>In<sub>3</sub> is shown in (Figure S8). Figure 9 (a) shows species distribution on Ni and NiIn as an example. At low coverage, acetylene is the dominant species on the reaction surface (Figure 9 (a)) and because of its high adsorption energy, it saturates the surface until 1 ML and, hence, poisons the catalysts.

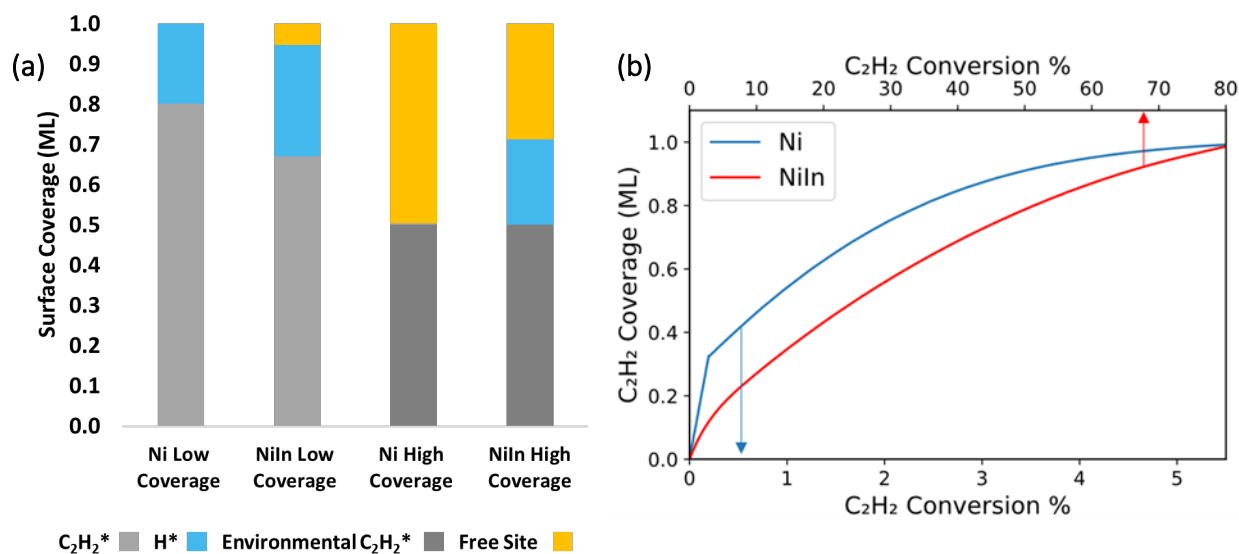
With regards to catalytic conversion, Figure 9 (b) shows that the low coverage assumption for Ni and NiIn resulted in rapid full coverage of the catalytic surface by C<sub>2</sub>H<sub>2</sub>, indicating that the reaction was limited by acetylene poisoning caused by the high adsorption energy, evaluated at low coverage. Ni showed minimal conversion (6%) as the coverage of acetylene on the surface was increasing until it reached 1.0 ML (Figure 9 (b) (bottom)). This contrasts with the reported experimental results, which show acetylene conversion on Ni to range between 35% and 100%.<sup>20,21,30</sup>

Figure 9 (b) (top) shows that surface poisoning happened at a slower rate in the case of NiIn allowing the reaction to proceed until 80% acetylene conversion in comparison to Ni (6%). This is simply related to the fact that acetylene is adsorbed more strongly on Ni than on NiIn. In the case of Ni<sub>3</sub>In, the reaction proceeded to completion (100% conversion), however, the coverage of acetylene continually increased as the reaction progressed, reaching 1 ML (Figure S9). Ultimately, acetylene poisoning was observed in all the low coverage simulations except in Ni<sub>2</sub>In<sub>3</sub> because of the very weak acetylene adsorption.

The high coverage kinetic simulation was performed using an initial coverage of 0.5 or 0.6 ML, which equates to 4 C<sub>2</sub>H<sub>2</sub> molecules for a surface with 8 active sites for Ni, Ni<sub>3</sub>In, NiIn, and 6 C<sub>2</sub>H<sub>2</sub> with 10 active sites for Ni<sub>2</sub>In<sub>3</sub>. 0.5 ML coverage corresponds to the pivotal point at which the adsorption free energy per molecule shifts from high to low, as illustrated in Figure 5. It is worth noting, however, that 0.5 ML coverage does not necessarily correspond to the most stable thermodynamic state, as additional molecules can still weakly adsorb to the surface. In addition, the choice of 0.5 ML as the initial coverage for the high coverage model, was justified a posteriori by the kinetic simulations.

The high coverage model showed no increase in acetylene coverage for the surfaces and maintained the initial coverage of 0.5 ML throughout the simulations (Figure 9 (a) and Figure S8). Ni showed a conversion value of 45%, which is compatible with the experimental values.<sup>20,21,30</sup> According to the high coverage model, hydrogen was covering a fraction of the surface on NiIn as shown in Figure 9 (a). Gibbs free energies of hydrogen and acetylene co-adsorbed on NiIn surface (Figure S10) show that acetylene adsorption was favored without accumulation of hydrogen on the surface which agrees with the microkinetic model.

The unchanged coverage at steady state, compared to the initial coverage of acetylene molecules stems from the weak differential adsorption energy (Table S16) and the enhanced desorption rates facilitated by the preadsorbed species on the surface. The different results obtained by the two models highlight the lack of consistency in the acetylene coverage when low coverage was assumed, in contrast to the self-consistent nature of the high coverage approach, which aligns with the initial conditions.



**Figure 9. (a)** Surface coverage distributions of main reaction species were taken at the same conversion value (40% C<sub>2</sub>H<sub>2</sub> conversion except for Ni at low coverage for which it was taken at 2.5% conversion because the reaction stopped before reaching 40%). 40% was selected as the benchmark conversion, as it represents the lowest conversion observed in most of the catalysts, at both low and high coverage models. Environmental C<sub>2</sub>H<sub>2</sub> corresponds to the initial 0.5 ML/0.6 ML coverage of acetylene considered for the simulations using the high coverage energy profiles, that can only access the remaining sites. **(b)** Coverage of acetylene

**as a function of acetylene conversion on Ni (bottom) and NiIn (top) using data at low coverage.**

Figure 10 shows the distribution of the products at the reactor outlet using the kinetic models established with energies obtained at low and high acetylene coverage. The ethylene levels presented in Figure 10 are the amount of ethylene generated during the reaction and do not account for the initial concentration of ethylene in the feed. NiIn exhibited the highest ethylene production in both models. NiIn and Ni<sub>2</sub>In<sub>3</sub> showed a significant decrease in ethane levels in contrast to Ni and Ni<sub>3</sub>In. However, this decrease in ethane production comes with a corresponding rise in the formation of oligomers (Figure 10(a-b)). This highlights the importance of considering the oligomerization reaction when assessing catalyst selectivity, rather than limiting selectivity to the amount of ethane produced.

The high selectivity to acetylene oligomerization on Ni<sub>2</sub>In<sub>3</sub> presents it as a potentially promising catalyst for C-C coupling reactions. This could be resulting from the weak binding energies of acetylene on the surface. It was proven by Lausche *et al.* that transition metals with weak binding energies exhibited larger adsorbate–adsorbate interactions in comparison to transition metals with strong binding energies.<sup>56</sup> The strong binding between the molecule and the catalyst surface makes it more difficult for the molecule to react with other molecules. This is because the energy required to break the bond between the molecule and the catalyst surface is greater for a strong bond compared to a weak bond.<sup>57</sup> Thus, increased selectivity for oligomers was observed on NiIn and Ni<sub>2</sub>In<sub>3</sub> (Figure 10).



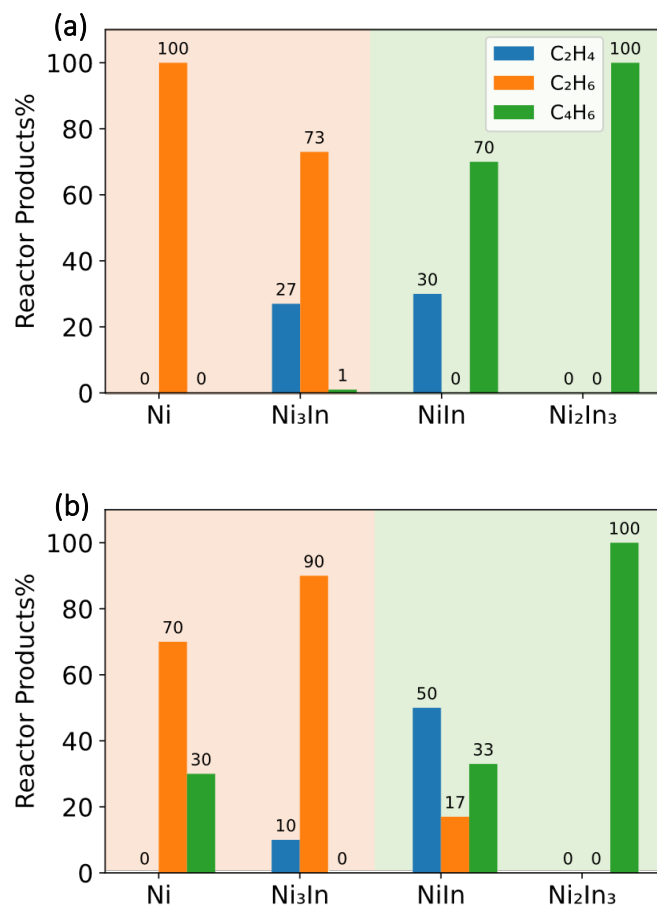


**Figure 10.** Calculated distribution of products at the reactor outlet at (a) low coverage and (b) high coverage. Feed composition (1:1:100 C<sub>2</sub>H<sub>2</sub>:H<sub>2</sub>:C<sub>2</sub>H<sub>4</sub>) at 433 K and 10 bar. The ethylene levels denote the amount of ethylene generated during the reaction and do not include the initial concentration of ethylene in the feed. Orange regions (left) indicate surfaces with high selectivity to ethane and green regions (right) indicate surfaces with high selectivity to butadiene.

Figure 11 presents the acetylene consumption rates and yield of ethylene calculated using data at low and high acetylene coverage. All values were calculated at a 40% conversion except for the Ni at low coverage because the reaction only proceeded to a 6% conversion. 40% was selected as the benchmark, as it represents the lowest conversion observed among the catalysts, at both low and high coverage models.

The highly negative ethylene yield on Ni shown in **Figure 11 (a-b)** is due to the rapid hydrogenation of ethylene in the feed on Ni active sites. The low activity of  $\text{Ni}_2\text{In}_3$  was attributed to the weak adsorption of acetylene and the substantial energy barriers for hydrogenation, even at high coverage as was discussed in the previous sections. In the low coverage model (**Figure 11 (a)**),  $\text{Ni}_3\text{In}$  was the most active catalyst with the highest ethylene yield. On the other hand, the most active catalyst and the highest ethylene yield in the high coverage model were Ni and  $\text{NiIn}$ , respectively (**Figure 11 (b)**). The microkinetic model using high coverage data showed that the presence of In on the catalytic surface decreased the rate of acetylene consumption, which is associated with the decrease in adsorption strength. A similar trend was found when alloying Pd with coinage metals.<sup>58</sup> Moreover, **Figure 11 (b)**, shows a tradeoff relationship between activity and selectivity. This relationship is not seen in **Figure 11 (a)** when the coverage effect was neglected.

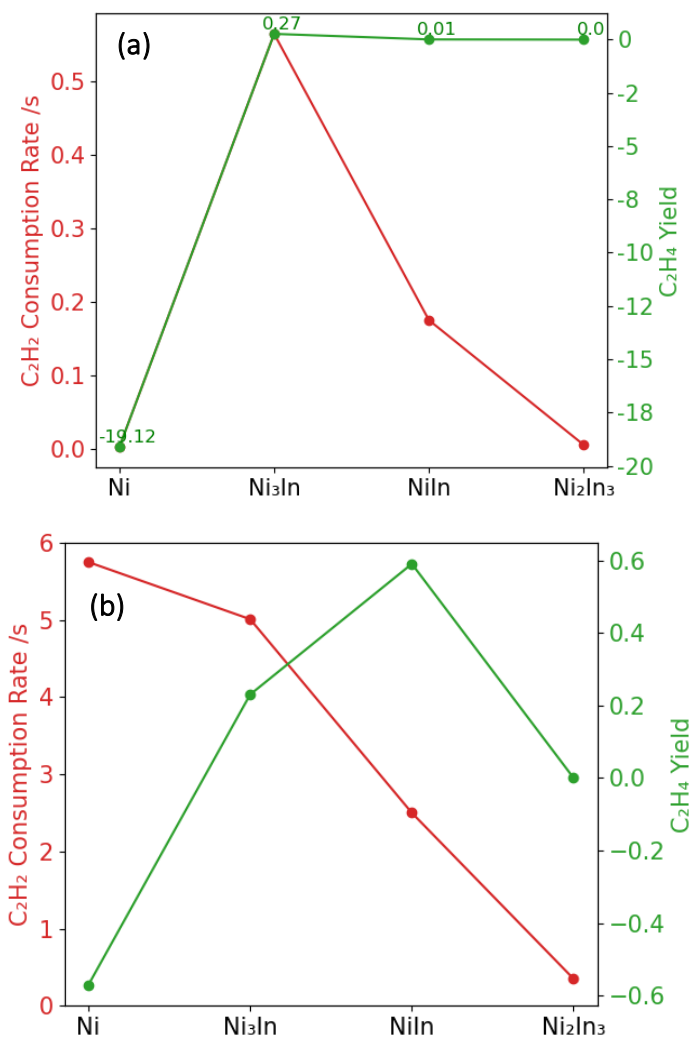


**Figure 11.** Acetylene consumption rates and yield of ethylene at 40% acetylene conversion using (a) low coverage energy data and (b) high coverage energy data. All values were calculated at a 40% conversion except for the Ni at low coverage because the reaction only proceeded to a 6% conversion. 40% was selected as the benchmark, as it represents the lowest conversion observed among the catalysts, at both low and high coverage models. A tradeoff relationship between activity and selectivity is observed when using the high coverage data. This relationship is not seen when the coverage effect was neglected.

Discrepancies in the literature regarding the origin of selectivity may be owed to the use of different feed compositions when evaluating catalysts. The results of the microkinetic simulations at high coverage, utilizing ethylene-rich feed (1:1:100 C<sub>2</sub>H<sub>2</sub>:H<sub>2</sub>:C<sub>2</sub>H<sub>4</sub>) in comparison to C<sub>2</sub>H<sub>2</sub> and H<sub>2</sub> feed only (1:1 C<sub>2</sub>H<sub>2</sub>:H<sub>2</sub>) are presented in **Figure 12 (a-b)**. The formation of C<sub>4</sub>H<sub>6</sub> was consistent when utilizing both feeds, which confirms that oligomers were primarily formed from acetylene C-C coupling reactions, in line with the isotopic labeling experimental results on Ni-Zn catalysts.<sup>20</sup> Experiments showed a ratio of 3:1 of the ethane produced from hydrogenating the ethylene in the feed to the ethane produced from the over-hydrogenation of acetylene.<sup>20</sup> This explains the C<sub>2</sub>H<sub>4</sub> consumption on Ni when using the (1:1:100 C<sub>2</sub>H<sub>2</sub>:H<sub>2</sub>:C<sub>2</sub>H<sub>4</sub>) feed (**Figure 12 (a)**). On the other hand, all surfaces showed minimal ethane formation and increased ethylene selectivity when utilizing the (1:1 C<sub>2</sub>H<sub>2</sub>:H<sub>2</sub>) feed (**Figure 12 (b)**) confirming that the primary source of ethane was the hydrogenation of the ethylene in the feed. Therefore, testing catalysts with pure acetylene may provide an inaccurate representation of the selectivity of the catalysts under actual reaction conditions. Understanding the origin of side products, in this case, ethane and oligomers, provides insight into the reaction mechanism by identifying the key intermediates and pathways contributing to their formation and, thus, guides future optimizations to reduce or eliminate their production.

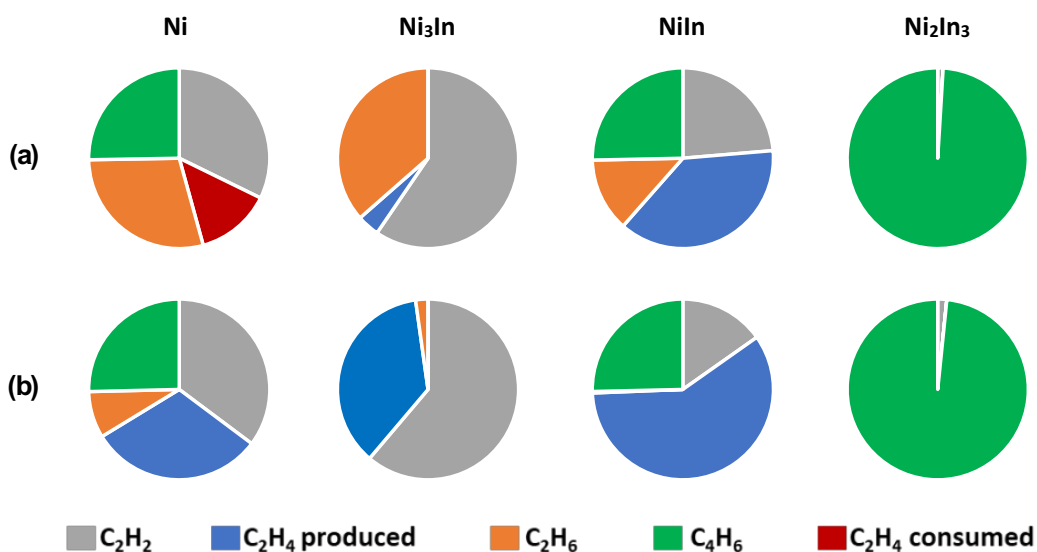


**Figure 12.** (a) Products distribution at the reactor outlet with a feed composition of (1:1:100 C<sub>2</sub>H<sub>2</sub>:H<sub>2</sub>:C<sub>2</sub>H<sub>4</sub>) at 10 bar and 433 K. (b) Products distribution at the reactor outlet in the absence of ethylene with a feed composition of (1:1 C<sub>2</sub>H<sub>2</sub>:H<sub>2</sub>) at 0.2 bar and 433 K. Significantly reduced levels of ethane formation were obtained in the absence of ethylene in the feed (b), in comparison to the results obtained with rich ethylene feed (a). These results were obtained using the high coverage model.

In summary, NiIn exhibited enhanced ethylene yield with reasonable activity regardless of the coverage model (Figure 10 and Figure 11) and feed composition (Figure 12) in comparison to Ni, Ni<sub>3</sub>In and Ni<sub>2</sub>In<sub>3</sub>. A remarkable ethylene selectivity was achieved (95%) on NiIn in the absence of ethylene in the feed and at an increased pressure of 20 bar (Figure S11). It is important to recognize that product distribution results do not depict the optimum performance of the catalysts, but rather, they provide an understanding of their relative performance under standardized reaction conditions. The reaction conditions could be optimized for each catalyst individually; however, this falls outside the scope of this study.

## 4. CONCLUSION

DFT-based reaction profiles and microkinetic simulations were used to describe the reaction chemistry of acetylene hydrogenation on Ni-In intermetallic catalysts. NiIn showed the highest ethylene yield among the studied catalysts. In comparison to Ni, Ni<sub>3</sub>In, and NiIn exhibited enhanced ethylene selectivity. While low ethane levels were formed on NiIn and Ni<sub>2</sub>In<sub>3</sub> compared to Ni and Ni<sub>3</sub>In, levels of C<sub>4</sub>H<sub>6</sub> were also observed, which highlights the importance of accounting for oligomerization reactions when applying a selectivity descriptor to screen catalysts.

The high adsorption energies at low coverage resulted in the surface being saturated with acetylene and blocking the reaction. On the other hand, the high coverage model showed that surfaces were not poisoned by acetylene and maintained the initial coverage throughout the simulations. The contrasting outcomes of the two models demonstrate the inconsistent nature of acetylene coverage when assuming low coverage, while the high coverage model was self-consistent and accurately reflected the initial conditions. Results from the high coverage microkinetic model showed that the presence of In on the catalytic surface decreased the rate of acetylene consumption and a trade-off relation between activity and selectivity was observed.

The effect of feed composition on catalysts selectivity was also investigated. Reduced ethane production was observed in the absence of ethylene in the feed which confirmed that the origin of ethane formation was primarily from ethylene hydrogenation rather than acetylene over hydrogenation. The results also showed that the formation of oligomers was not impacted by the presence or absence of ethylene in the feed, thereby confirming that the source of oligomerization was acetylene. The study provides insights to better understand and evaluate the selectivity of catalysts and serves as a step towards developing a competitive alternative to the current Pd-Ag industrial catalyst for the semi-hydrogenation of alkynes.

## **5. SUPPORTING INFORMATION**

Ni-In phase diagram, density of states calculations, details of bulk unit cells, surface facets calculations, adsorption sites, optimized structures, and additional microkinetic modeling results.

## **6. ACKNOWLEDGEMENT**

Z.A. gratefully acknowledges Saudi Aramco for their funding. This work was supported by the Supercomputing Laboratory at King Abdullah University of Science & Technology (KAUST) in Thuwal, Saudi Arabia, the Extreme Science and Engineering Discovery Environment (XSEDE) Expanse and Bridges-2 clusters at San Diego Supercomputer Center through allocation TG-CHE170060 and the UCLA Institute of Digital Research and Education (IDRE) for computational resources on the UCLA Hoffman2 cluster.

## 7. REFERENCES

- (1) Haribal, V. P.; Chen, Y.; Neal, L.; Li, F. Intensification of Ethylene Production from Naphtha via a Redox Oxy-Cracking Scheme: Process Simulations and Analysis. *Engineering* **2018**, *4* (5), 714–721. <https://doi.org/10.1016/J.ENG.2018.08.001>.
- (2) Bos, A. N. R.; Westerterp, K. R. Mechanism and Kinetics of the Selective Hydrogenation of Ethyne and Ethene. *Chemical Engineering and Processing: Process Intensification* **1993**, *32* (1), 1–7. [https://doi.org/10.1016/0255-2701\(93\)87001-B](https://doi.org/10.1016/0255-2701(93)87001-B).
- (3) Takht Ravanchi, M.; Sahebdehfar, S.; Komeili, S. Acetylene Selective Hydrogenation: A Technical Review on Catalytic Aspects. *Reviews in Chemical Engineering* **2017**, *34* (2), 215–237. <https://doi.org/10.1515/revce-2016-0036>.
- (4) Urmès, C.; Schweitzer, J. M.; Cabiac, A.; Schuurman, Y. Kinetic Study of the Selective Hydrogenation of Acetylene over Supported Palladium under Tail-End Conditions. *Catalysts* **2019**, *9* (2). <https://doi.org/10.3390/catal9020180>.
- (5) Rao, D. M.; Zhang, S. T.; Li, C. M.; Chen, Y. Di; Pu, M.; Yan, H.; Wei, M. The Reaction Mechanism and Selectivity of Acetylene Hydrogenation over Ni-Ga Intermetallic Compound Catalysts: A Density Functional Theory Study. *Dalton Transactions* **2018**, *47* (12), 4198–4208. <https://doi.org/10.1039/c7dt04726f>.
- (6) Armbrüster, M. Intermetallic Compounds in Catalysis—a Versatile Class of Materials Meets Interesting Challenges. *Science and Technology of Advanced Materials* **2020**, *21* (1), 303–322. <https://doi.org/10.1080/14686996.2020.1758544>.
- (7) Rößner, L.; Armbrüster, M. Electrochemical Energy Conversion on Intermetallic Compounds: A Review. *ACS Catalysis* **2019**, *9* (3), 2018–2062. <https://doi.org/10.1021/acscatal.8b04566>.
- (8) Yang, T.; Feng, Y.; Ma, R.; Li, Q.; Yan, H.; Liu, Y.; He, Y.; Miller, J. T.; Li, D. Improvement of Selectivity in Acetylene Hydrogenation with Comparable Activity over Ordered PdCu Catalysts Induced by Post-Treatment. *ACS Applied Materials and Interfaces* **2021**, *13* (1), 706–716. <https://doi.org/10.1021/acsami.0c19329>.
- (9) Furukawa, S.; Komatsu, T. Intermetallic Compounds: Promising Inorganic Materials for Well-Structured and Electronically Modified Reaction Environments for Efficient Catalysis. *ACS Catalysis* **2017**, *7* (1), 735–765. <https://doi.org/10.1021/acscatal.6b02603>.
- (10) Antolini, E. Alloy vs. Intermetallic Compounds: Effect of the Ordering on the Electrocatalytic Activity for Oxygen Reduction and the Stability of Low Temperature Fuel Cell Catalysts. *Applied Catalysis B: Environmental* **2017**, *217*, 201–213. <https://doi.org/10.1016/j.apcatb.2017.05.081>.
- (11) Dasgupta, A.; Rioux, R. M. Intermetallics in Catalysis: An Exciting Subset of Multimetallic Catalysts. *Catalysis Today* **2019**, *330*, 2–15. <https://doi.org/10.1016/j.cattod.2018.05.048>.
- (12) Luo, Y.; Alarcón Villaseca, S.; Friedrich, M.; Teschner, D.; Knop-Gericke, A.; Armbrüster, M. Addressing Electronic Effects in the Semi-Hydrogenation of Ethyne by InPd<sub>2</sub> and Intermetallic Ga-Pd Compounds. *Journal of Catalysis* **2016**, *338*, 265–272. <https://doi.org/10.1016/j.jcat.2016.03.025>.
- (13) Vignola, E.; Steinmann, S. N.; Le Mapihan, K.; Vandegheuchte, B. D.; Curulla, D.; Sautet, P. Acetylene Adsorption on Pd-Ag Alloys: Evidence for Limited Island Formation and Strong Reverse

- Segregation from Monte Carlo Simulations. *Journal of Physical Chemistry C* **2018**, *122* (27), 15456–15463. <https://doi.org/10.1021/acs.jpcc.8b04108>.
- (14) Dasgupta, A.; He, H.; Gong, R.; Shang, S. L.; Zimmerer, E. K.; Meyer, R. J.; Liu, Z. K.; Janik, M. J.; Rioux, R. M. Atomic Control of Active-Site Ensembles in Ordered Alloys to Enhance Hydrogenation Selectivity. *Nature Chemistry* **2022**, *14* (5), 523–529. <https://doi.org/10.1038/s41557-021-00855-3>.
- (15) Wegener, E. C.; Bukowski, B. C.; Yang, D.; Wu, Z.; Kropf, A. J.; Delgass, W. N.; Greeley, J.; Zhang, G.; Miller, J. T. Intermetallic Compounds as an Alternative to Single-Atom Alloy Catalysts: Geometric and Electronic Structures from Advanced X-Ray Spectroscopies and Computational Studies. *ChemCatChem* **2020**, *12* (5), 1325–1333. <https://doi.org/10.1002/cctc.201901869>.
- (16) Osswald, J.; Kovnir, K.; Armbrüster, M.; Giedigkeit, R.; Jentoft, R. E.; Wild, U.; Grin, Y.; Schlögl, R. Palladium-Gallium Intermetallic Compounds for the Selective Hydrogenation of Acetylene. Part II: Surface Characterization and Catalytic Performance. *Journal of Catalysis* **2008**, *258* (1), 219–227. <https://doi.org/10.1016/j.jcat.2008.06.014>.
- (17) Xu, L.; Stangland, E. E.; Mavrikakis, M. Ethylene versus Ethane: A DFT-Based Selectivity Descriptor for Efficient Catalyst Screening. *Journal of Catalysis* **2018**, *362*, 18–24. <https://doi.org/10.1016/j.jcat.2018.03.019>.
- (18) Cao, Y.; Sui, Z.; Zhu, Y.; Zhou, X.; Chen, D. Selective Hydrogenation of Acetylene over Pd-In/Al<sub>2</sub>O<sub>3</sub> Catalyst: Promotional Effect of Indium and Composition-Dependent Performance. *ACS Catalysis* **2017**, *7* (11), 7835–7846. <https://doi.org/10.1021/acscatal.7b01745>.
- (19) Kim, W. J.; Moon, S. H. Modified Pd Catalysts for the Selective Hydrogenation of Acetylene. *Catalysis Today* **2012**, *185* (1), 2–16. <https://doi.org/10.1016/j.cattod.2011.09.037>.
- (20) Spanjers, C. S.; Held, J. T.; Jones, M. J.; Stanley, D. D.; Sim, R. S.; Janik, M. J.; Rioux, R. M. Zinc Inclusion to Heterogeneous Nickel Catalysts Reduces Oligomerization during the Semi-Hydrogenation of Acetylene. *Journal of Catalysis* **2014**, *316*, 164–173. <https://doi.org/10.1016/j.jcat.2014.05.007>.
- (21) Zhou, S.; Kang, L.; Zhou, X.; Xu, Z.; Zhu, M. Pure Acetylene Semihydrogenation over Ni–Cu Bimetallic Catalysts: Effect of the Cu/Ni Ratio on Catalytic Performance. *Nanomaterials* **2020**, *10* (3), 1–12. <https://doi.org/10.3390/nano10030509>.
- (22) Guo, J.; Wang, Z.; Li, J.; Wang, Z. In-Ni Intermetallic Compounds Derived from Layered Double Hydroxides as Efficient Catalysts toward the Reverse Water Gas Shift Reaction. *ACS Catalysis* **2022**, *12* (7), 4026–4036. <https://doi.org/10.1021/acscatal.2c00671>.
- (23) Li, C.; Chen, Y.; Zhang, S.; Xu, S.; Zhou, J.; Wang, F.; Wei, M.; Evans, D. G.; Duan, X. Ni-In Intermetallic Nanocrystals as Efficient Catalysts toward Unsaturated Aldehydes Hydrogenation. *Chemistry of Materials* **2013**, *25* (19), 3888–3896. <https://doi.org/10.1021/cm4021832>.
- (24) Song, Y.; Laursen, S. Control of Surface Reactivity towards Unsaturated C–C Bonds and H over Ni-Based Intermetallic Compounds in Semi-Hydrogenation of Acetylene. *Journal of Catalysis* **2019**, *372*, 151–162. <https://doi.org/10.1016/j.jcat.2019.02.018>.
- (25) Wang, J.; Xu, H.; Che, C.; Zhu, J.; Cheng, D. Rational Design of PdAg Catalysts for Acetylene Selective Hydrogenation via Structural Descriptor-Based Screening Strategy. *ACS Catalysis* **2022**, *13*, 433–444. <https://doi.org/10.1021/acscatal.2c05498>.



- (26) Studt, F.; Abild-Pedersen, F.; Bligaard, T.; Sørensen, R. Z.; Christensen, C. H.; Nørskov, J. K. Identification of Non-Precious Metal Alloy Catalysts for Selective Hydrogenation of Acetylene. *Science* **2008**, *320* (5881), 1320–1322. <https://doi.org/10.1126/science.1156660>.
- (27) Zhao, J.; Zha, S.; Mu, R.; Zhao, Z. J.; Gong, J. Coverage Effect on the Activity of the Acetylene Semihydrogenation over Pd-Sn Catalysts: A Density Functional Theory Study. *Journal of Physical Chemistry C* **2018**, *122* (11), 6005–6013. <https://doi.org/10.1021/acs.jpcc.7b11394>.
- (28) Xie, W.; Xu, J.; Ding, Y.; Hu, P. Quantitative Studies of the Key Aspects in Selective Acetylene Hydrogenation on Pd(111) by Microkinetic Modeling with Coverage Effects and Molecular Dynamics. *ACS Catalysis* **2021**, *11* (7), 4094–4106. <https://doi.org/10.1021/acscatal.0c05345>.
- (29) Huang, F.; Peng, M.; Chen, Y.; Cai, X.; Qin, X.; Wang, N.; Xiao, D.; Jin, L.; Wang, G.; Wen, X. D.; Liu, H.; Ma, D. Low-Temperature Acetylene Semi-Hydrogenation over the Pd<sub>1</sub>-Cu<sub>1</sub>Dual-Atom Catalyst. *Journal of the American Chemical Society* **2022**, *144* (40), 18485–18493. <https://doi.org/10.1021/jacs.2c07208>.
- (30) Chen, Y.; Chen, J. Selective Hydrogenation of Acetylene on SiO<sub>2</sub> Supported Ni-In Bimetallic Catalysts: Promotional Effect of In. *Applied Surface Science* **2016**, *387*, 16–27. <https://doi.org/10.1016/j.apsusc.2016.06.067>.
- (31) Okamoto, H.; Schlesinger, M. E.; Mueller, E. M. In (Indium) Binary Alloy Phase Diagrams. In *Alloy Phase Diagrams*; ASM International, 2016; Vol. 3, pp 429–446. <https://doi.org/10.31399/asm.hb.v03.a0006171>.
- (32) Jain, A.; Ong, S. P.; Hautier, G.; Chen, W.; Richards, W. D.; Dacek, S.; Cholia, S.; Gunter, D.; Skinner, D.; Ceder, G.; Persson, K. A. Commentary: The Materials Project: A Materials Genome Approach to Accelerating Materials Innovation. *APL Materials*. 2013, p 11002. <https://doi.org/10.1063/1.4812323>.
- (33) Kresse, G.; Furthmüller, J. Efficiency of *Ab-Initio* Total Energy Calculations for Metals and Semiconductors Using a Plane-Wave Basis Set. *Computational Materials Science* **1996**, *6* (1), 15–50. [https://doi.org/10.1016/0927-0256\(96\)00008-0](https://doi.org/10.1016/0927-0256(96)00008-0).
- (34) Kresse, G. Efficient Iterative Schemes for *Ab Initio* Total-Energy Calculations Using a Plane-Wave Basis Set. *Physical Review B* **1996**, *54* (16), 11169–11186. <https://doi.org/10.1103/PhysRevB.54.11169>.
- (35) Kresse, G.; Joubert, D. From Ultrasoft Pseudopotentials to the Projector Augmented-Wave Method. *Physical Review B* **1999**, *59* (3), 1758–1775. <https://doi.org/10.1103/PhysRevB.59.1758>.
- (36) Blochl, P. E. Augmented-wave. *PHYSICAL REVIEW B* **1994**, *50*, 17953–17979. <https://doi.org/10.1103/physrevb.50.17953>.
- (37) Perdew, J. P.; Burke, K.; Ernzerhof, M. Generalized Gradient Approximation Made Simple. *Physical Review Letters* **1996**, *77* (18), 3865–3868. <https://doi.org/10.1103/PhysRevLett.77.3865>.
- (38) Grimme, S.; Antony, J.; Ehrlich, S.; Krieg, H. A Consistent and Accurate *Ab Initio* Parametrization of Density Functional Dispersion Correction (DFT-D) for the 94 Elements H-Pu. *J. Chem. Phys* **2010**, *132*, 154104. <https://doi.org/10.1063/1.3382344>.
- (39) Grimme, S.; Ehrlich, S.; Goerigk, L. Effect of the Damping Function in Dispersion Corrected Density Functional Theory. *Journal of Computational Chemistry* **2011**, *32* (7), 1456–1465.

- <https://doi.org/10.1002/jcc.21759>.
- (40) Cao, Y.; Zhang, H.; Ji, S.; Sui, Z.; Jiang, Z.; Wang, D.; Zaera, F.; Zhou, X.; Duan, X.; Li, Y. Adsorption Site Regulation to Guide Atomic Design of Ni–Ga Catalysts for Acetylene Semi-Hydrogenation. *Angewandte Chemie* **2020**, *132* (28), 11647–11652. <https://doi.org/10.1002/ange.202004966>.
- (41) Yang, H.; Whitten, J. L. Dissociative Adsorption of H<sub>2</sub> on Ni(111). *The Journal of Chemical Physics* **1993**, *98* (6), 5039–5049. <https://doi.org/10.1063/1.464958>.
- (42) Cheng, Y.; Song, Y.; Zhang, Y. A Systematic Investigation of the Catalytic Performances of Monolayer Carbon Nitride Nanosheets C<sub>1</sub>–xN<sub>x</sub>. *Physical Chemistry Chemical Physics* **2020**, *22* (12), 6772–6782. <https://doi.org/10.1039/D0CP00319K>.
- (43) Hjorth Larsen, A.; Jørgen Mortensen, J.; Blomqvist, J.; Castelli, I. E.; Christensen, R.; Duřak, M.; Friis, J.; Groves, M. N.; Hammer, B.; Hargus, C.; Hermes, E. D.; Jennings, P. C.; Bjerre Jensen, P.; Kermode, J.; Kitchin, J. R.; Leonhard Kolsbjerg, E.; Kubal, J.; Kaasbjerg, K.; Lysgaard, S.; Bergmann Maronsson, J.; Maxson, T.; Olsen, T.; Pastewka, L.; Peterson, A.; Rostgaard, C.; Schiøtz, J.; Schütt, O.; Strange, M.; Thygesen, K. S.; Vegge, T.; Vilhelmsen, L.; Walter, M.; Zeng, Z.; Jacobsen, K. W. The Atomic Simulation Environment—a Python Library for Working with Atoms. *Journal of Physics: Condensed Matter* **2017**, *29* (27), 273002. <https://doi.org/10.1088/1361-648X/aa680e>.
- (44) Henkelman, G.; Uberuaga, B. P.; Jónsson, H. Climbing Image Nudged Elastic Band Method for Finding Saddle Points and Minimum Energy Paths. *Journal of Chemical Physics* **2000**, *113* (22), 9901–9904. <https://doi.org/10.1063/1.1329672>.
- (45) Henkelman, G.; Jónsson, H. A Dimer Method for Finding Saddle Points on High Dimensional Potential Surfaces Using Only First Derivatives. *Journal of Chemical Physics* **1999**, *111* (15), 7010–7022. <https://doi.org/10.1063/1.480097>.
- (46) Motagamwala, A. H.; Dumesic, J. A. Microkinetic Modeling: A Tool for Rational Catalyst Design. *Chemical Reviews*. 2021, pp 1049–1076. <https://doi.org/10.1021/acs.chemrev.0c00394>.
- (47) Gokhale, A. A.; Kandoi, S.; Greeley, J. P.; Mavrikakis, M.; Dumesic, J. A. Molecular-Level Descriptions of Surface Chemistry in Kinetic Models Using Density Functional Theory. *Chemical Engineering Science* **2004**, *59* (22–23), 4679–4691. <https://doi.org/10.1016/j.ces.2004.09.038>.
- (48) Wang, T.; Ibañez, J.; Wang, K.; Fang, L.; Sabbe, M.; Michel, C.; Paul, S.; Pera-Titus, M.; Sautet, P. Rational Design of Selective Metal Catalysts for Alcohol Amination with Ammonia. *Nature Catalysis* **2019**, *2* (9), 773–779. <https://doi.org/10.1038/s41929-019-0327-2>.
- (49) Zhang, W.-B.; Chen, C.; Zhang, Y. Equilibrium Crystal Shape of Ni from First Principles. **2013**. <https://doi.org/10.1021/jp404569m>.
- (50) Yang, K.; Li, Y.; Wang, R.; Li, Q.; Huang, B.; Guo, X.; Zhu, Z.; Su, T.; Lü, H. Synthesis of Dual-Active-Sites Ni–Ni<sub>2</sub>In Catalysts for Selective Hydrogenation of Furfural to Furfuryl Alcohol. *Fuel* **2022**, *325* (June), 124898. <https://doi.org/10.1016/j.fuel.2022.124898>.
- (51) Vignola, E.; Steinmann, S. N.; Al Farra, A.; Vandegehuchte, B. D.; Curulla, D.; Sautet, P. Evaluating the Risk of C–C Bond Formation during Selective Hydrogenation of Acetylene on Palladium. *ACS Catalysis* **2018**, *8* (3), 1662–1671. <https://doi.org/10.1021/acscatal.7b03752>.
- (52) Qi, Y.; Wang, B.; Fan, M.; Li, D.; Zhang, R. C<sub>2</sub>H<sub>2</sub> Semi-Hydrogenation on the Metal M (M = Cu, Ag, Au) Alloyed Single-Atom Pd Catalysts: Effects of Pd Coordination Number and Environment on

- the Catalytic Performance. *Chemical Engineering Science* **2021**, *243*, 116786. <https://doi.org/10.1016/j.ces.2021.116786>.
- (53) Rao, D. M.; Sun, T.; Yang, Y. Sen; Yin, P.; Pu, M.; Yan, H.; Wei, M. Theoretical Study on the Reaction Mechanism and Selectivity of Acetylene Semi-Hydrogenation on Ni-Sn Intermetallic Catalysts. *Physical Chemistry Chemical Physics* **2019**, *21* (3), 1384–1392. <https://doi.org/10.1039/c8cp06032k>.
- (54) López, N.; Vargas-Fuentes, C. Promoters in the Hydrogenation of Alkynes in Mixtures: Insights from Density Functional Theory. *Chemical Communications* **2012**, *48* (10), 1379–1391. <https://doi.org/10.1039/c1cc14922a>.
- (55) Xie, W.; Hu, P. Influence of Surface Defects on Activity and Selectivity: A Quantitative Study of Structure Sensitivity of Pd Catalysts for Acetylene Hydrogenation. *Catalysis Science and Technology* **2021**, *11* (15), 5212–5222. <https://doi.org/10.1039/d1cy00665g>.
- (56) Lausche, A. C.; Medford, A. J.; Khan, T. S.; Xu, Y.; Bligaard, T.; Abild-Pedersen, F.; Nørskov, J. K.; Studt, F. On the Effect of Coverage-Dependent Adsorbate-Adsorbate Interactions for CO Methanation on Transition Metal Surfaces. *Journal of Catalysis* **2013**, *307*, 275–282. <https://doi.org/10.1016/j.jcat.2013.08.002>.
- (57) Aljama, H.; Abild-Pedersen, F. Accessing the C-C Transition State Energy on Transition Metals. *Physical Chemistry Chemical Physics* **2019**, *21* (45), 25328–25333. <https://doi.org/10.1039/c9cp04897a>.
- (58) Huang, Y.; Chen, Z. X. Alloying Effect on the C–C Coupling Reactions in Acetylene Hydrogenation by Palladium-Coinage Metal Alloys, a DFT Study and Microkinetic Modeling. *Applied Surface Science* **2022**, *575* (September 2021), 151513. <https://doi.org/10.1016/j.apsusc.2021.151513>.

